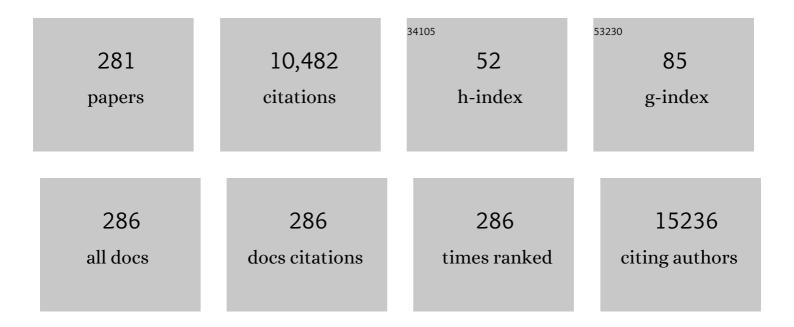
## Aart Johannes Nederveen

List of Publications by Year in descending order

Source: https://exaly.com/author-pdf/5018425/publications.pdf Version: 2024-02-01



#	Article	IF	CITATIONS
1	Oxidized Phospholipids on Lipoprotein(a) Elicit Arterial Wall Inflammation and an Inflammatory Monocyte Response in Humans. Circulation, 2016, 134, 611-624.	1.6	396
2	Deep brain stimulation restores frontostriatal network activity in obsessive-compulsive disorder. Nature Neuroscience, 2013, 16, 386-387.	14.8	379
3	RECOORD: A recalculated coordinate database of 500+ proteins from the PDB using restraints from the BioMagResBank. Proteins: Structure, Function and Bioinformatics, 2005, 59, 662-672.	2.6	323
4	Assessment of Hepatic Steatosis in Patients Undergoing Liver Resection: Comparison of US, CT, T1-weighted Dual-Echo MR Imaging, and Point-resolved <sup>1</sup> H MR Spectroscopy. Radiology, 2010, 256, 159-168.	7.3	286
5	Cerebral hyporesponsiveness and cognitive impairment 10 years after chemotherapy for breast cancer. Human Brain Mapping, 2011, 32, 1206-1219.	3.6	243
6	Mipomersen, an apolipoprotein B synthesis inhibitor, lowers low-density lipoprotein cholesterol in high-risk statin-intolerant patients: a randomized, double-blind, placebo-controlled trial. European Heart Journal, 2012, 33, 1142-1149.	2.2	171
7	Clinical feasibility study for the use of implanted gold seeds in the prostate as reliable positioning markers during megavoltage irradiation. Radiotherapy and Oncology, 2003, 67, 295-302.	0.6	162
8	Measurements and clinical consequences of prostate motion during a radiotherapy fraction. International Journal of Radiation Oncology Biology Physics, 2002, 53, 206-214.	0.8	147
9	Upper and extra-motoneuron involvement in early motoneuron disease: a diffusion tensor imaging study. Brain, 2011, 134, 1211-1228.	7.6	135
10	Techniques and applications of skeletal muscle diffusion tensor imaging: A review. Journal of Magnetic Resonance Imaging, 2016, 43, 773-788.	3.4	135
11	Accuracy and precision of pseudo-continuous arterial spin labeling perfusion during baseline and hypercapnia: A head-to-head comparison with 150 H2O positron emission tomography. NeuroImage, 2014, 92, 182-192.	4.2	133
12	Structural, functional and molecular imaging of the brain in primary focal dystonia—A review. NeuroImage, 2011, 56, 1011-1020.	4.2	132
13	Volumetric arterial wall shear stress calculation based on cine phase contrast MRI. Journal of Magnetic Resonance Imaging, 2015, 41, 505-516.	3.4	128
14	Intra- and Multicenter Reproducibility of Pulsed, Continuous and Pseudo-Continuous Arterial Spin Labeling Methods for Measuring Cerebral Perfusion. Journal of Cerebral Blood Flow and Metabolism, 2011, 31, 1706-1715.	4.3	127
15	Prednisolone-containing liposomes accumulate in human atherosclerotic macrophages upon intravenous administration. Nanomedicine: Nanotechnology, Biology, and Medicine, 2015, 11, 1039-1046.	3.3	127
16	N-Acetylcysteine Normalizes Glutamate Levels in Cocaine-Dependent Patients: A Randomized Crossover Magnetic Resonance Spectroscopy Study. Neuropsychopharmacology, 2012, 37, 2143-2152.	5.4	126
17	Neuroimaging essentials in essential tremor: A systematic review. Neurolmage: Clinical, 2014, 5, 217-231.	2.7	117
18	Hepatic Diacylglycerol-Associated Protein Kinase Cε Translocation Links Hepatic Steatosis to Hepatic Insulin Resistance in Humans, Cell Reports, 2017, 19, 1997-2004.	6.4	117

#	Article	IF	CITATIONS
19	Comparison of megavoltage position verification for prostate irradiation based on bony anatomy and implanted fiducials. Radiotherapy and Oncology, 2003, 68, 81-88.	0.6	111
20	Hypercaloric diets with increased meal frequency, but not meal size, increase intrahepatic triglycerides: A randomized controlled trial. Hepatology, 2014, 60, 545-553.	7.3	110
21	Muscle Changes Detected with Diffusion-Tensor Imaging after Long-Distance Running. Radiology, 2015, 274, 548-562.	7.3	110
22	DTI of human skeletal muscle: the effects of diffusion encoding parameters, signalâ€toâ€noise ratio and <i>T</i> <sub>2</sub> on tensor indices and fiber tracts. NMR in Biomedicine, 2013, 26, 1339-1352.	2.8	106
23	Effect of apolipoprotein-B synthesis inhibition on liver triglyceride content in patients with familial hypercholesterolemia. Journal of Lipid Research, 2010, 51, 1057-1062.	4.2	102
24	Diffusionâ€ŧensor MRI reveals the complex muscle architecture of the human forearm. Journal of Magnetic Resonance Imaging, 2012, 36, 237-248.	3.4	101
25	Pixel-by-pixel analysis of DCE MRI curve patterns and an illustration of its application to the imaging of the musculoskeletal system. Magnetic Resonance Imaging, 2007, 25, 604-612.	1.8	92
26	DRESS: a database of REfined solution NMR structures. Proteins: Structure, Function and Bioinformatics, 2004, 55, 483-486.	2.6	91
27	Non-invasive evaluation of liver fibrosis: a comparison of ultrasound-based transient elastography and MR elastography in patients with viral hepatitis B and C. European Radiology, 2014, 24, 638-648.	4.5	90
28	Exome Sequencing and Directed Clinical Phenotyping Diagnose Cholesterol Ester Storage Disease Presenting as Autosomal Recessive Hypercholesterolemia. Arteriosclerosis, Thrombosis, and Vascular Biology, 2013, 33, 2909-2914.	2.4	87
29	CSI-EPT: A Contrast Source Inversion Approach for Improved MRI-Based Electric Properties Tomography. IEEE Transactions on Medical Imaging, 2015, 34, 1788-1796.	8.9	86
30	Thresholds for Arterial Wall Inflammation Quantified by 18F-FDG PET Imaging. JACC: Cardiovascular Imaging, 2016, 9, 1198-1207.	5.3	81
31	ExploreASL: An image processing pipeline for multi-center ASL perfusion MRI studies. NeuroImage, 2020, 219, 117031.	4.2	80
32	MR Spectroscopy–derived Proton Density Fat Fraction Is Superior to Controlled Attenuation Parameter for Detecting and Grading Hepatic Steatosis. Radiology, 2018, 286, 547-556.	7.3	79
33	In Vivo Quantification of Carotid Artery Wall Dimensions. Circulation: Cardiovascular Imaging, 2009, 2, 235-242.	2.6	78
34	Determinants of resting cerebral blood flow in sickle cell disease. American Journal of Hematology, 2016, 91, 912-917.	4.1	76
35	The spatial coefficient of variation in arterial spin labeling cerebral blood flow images. Journal of Cerebral Blood Flow and Metabolism, 2017, 37, 3184-3192.	4.3	76
36	Effect of open-label infusion of an apoA-I-containing particle (CER-001) on RCT and artery wall thickness in patients with FHA. Journal of Lipid Research, 2015, 56, 703-712.	4.2	73

Aart Johannes Nederveen

#	Article	IF	CITATIONS
37	Multi-vendor reliability of arterial spin labeling perfusion MRI using a near-identical sequence: Implications for multi-center studies. NeuroImage, 2015, 113, 143-152.	4.2	72
38	Donor Fecal Microbiota Transplantation Alters Gut Microbiota and Metabolites in Obese Individuals With Steatohepatitis. Hepatology Communications, 2020, 4, 1578-1590.	4.3	71
39	Skeletal muscle diffusion tensorâ€MRI fiber tracking: rationale, data acquisition and analysis methods, applications and future directions. NMR in Biomedicine, 2017, 30, e3563.	2.8	68
40	A methodology to detect abnormal relative wall shear stress on the full surface of the thoracic aorta using four-dimensional flow MRI. Magnetic Resonance in Medicine, 2015, 73, 1216-1227.	3.0	67
41	Reproducibility of 3.0 Tesla magnetic resonance spectroscopy for measuring hepatic fat content. Journal of Magnetic Resonance Imaging, 2009, 30, 444-448.	3.4	66
42	Inter-Vendor Reproducibility of Pseudo-Continuous Arterial Spin Labeling at 3 Tesla. PLoS ONE, 2014, 9, e104108.	2.5	66
43	Wall shear stress estimated with phase contrast MRI in an in vitro and in vivo intracranial aneurysm. Journal of Magnetic Resonance Imaging, 2013, 38, 876-884.	3.4	65
44	Cortical Microinfarcts Detected In Vivo on 3 Tesla MRI. Stroke, 2015, 46, 255-257.	2.0	62
45	ABCA1 mutation carriers with low high-density lipoprotein cholesterol are characterized by a larger atherosclerotic burden. European Heart Journal, 2013, 34, 286-291.	2.2	61
46	NMR Relaxation and Internal Dynamics of Ubiquitin from a 0.2 μs MD Simulation. Journal of Chemical Theory and Computation, 2005, 1, 363-374.	5.3	60
47	Cerebral Perfusion Measurements in Elderly with Hypertension Using Arterial Spin Labeling. PLoS ONE, 2015, 10, e0133717.	2.5	60
48	Cholesterol Acyltransferase Gene Mutations Have Accelerated Atherogenesis as Assessed by Carotid 3.0-T Magnetic Resonance Imaging. Journal of the American College of Cardiology, 2011, 58, 2481-2487.	2.8	58
49	Arterial spin labeling measurement of cerebral perfusion in children with sickle cell disease. Journal of Magnetic Resonance Imaging, 2012, 35, 779-787.	3.4	58
50	Wall shear stress calculations based on 3D cine phase contrast MRI and computational fluid dynamics: a comparison study in healthy carotid arteries. NMR in Biomedicine, 2014, 27, 826-834.	2.8	56
51	US Cannot Be Used to Predict the Presence or Severity of Hepatic Steatosis in Severely Obese Adolescents. Radiology, 2012, 262, 327-334.	7.3	55
52	Volume of white matter hyperintensities is an independent predictor of intelligence quotient and processing speed in children with sickle cell disease. British Journal of Haematology, 2015, 168, 553-556.	2.5	55
53	Prenatal famine exposure has sex-specific effects on brain size. Brain, 2016, 139, 2136-2142.	7.6	54
54	Evaluation of ultrasmall superparamagnetic iron-oxide (USPIO) enhanced MRI with ferumoxytol to quantify arterial wall inflammation. Atherosclerosis, 2017, 263, 211-218.	0.8	53

#	Article	IF	CITATIONS
55	Treatment with Anaerobutyricum soehngenii: a pilot study of safety and dose–response effects on glucose metabolism in human subjects with metabolic syndrome. Npj Biofilms and Microbiomes, 2020, 6, 16.	6.4	53
56	HDL mimetic CER-001 targets atherosclerotic plaques in patients. Atherosclerosis, 2016, 251, 381-388.	0.8	51
57	Diagnostic accuracy of MRI and ultrasound in chronic immune-mediated neuropathies. Neurology, 2020, 94, e62-e74.	1.1	51
58	BioMagResBank databases DOCR and FRED containing converted and filtered sets of experimental NMR restraints and coordinates from over 500 protein PDB structures. Journal of Biomolecular NMR, 2005, 32, 1-12.	2.8	50
59	Noninvasive Differentiation between Hepatic Steatosis and Steatohepatitis with MR Imaging Enhanced with USPIOs in Patients with Nonalcoholic Fatty Liver Disease: A Proof-of-Concept Study. Radiology, 2016, 278, 782-791.	7.3	50
60	Multiâ€center evaluation of stability and reproducibility of quantitative MRI measures in healthy calf muscles. NMR in Biomedicine, 2019, 32, e4119.	2.8	50
61	Infusion of donor feces affects the gut–brain axis in humans with metabolic syndrome. Molecular Metabolism, 2020, 42, 101076.	6.5	50
62	Reproducibility of diffusion tensor imaging in human forearm muscles at 3.0 T in a clinical setting. Magnetic Resonance in Medicine, 2010, 64, 1182-1190.	3.0	49
63	Feasibility of Electric Property Tomography of pelvic tumors at 3T. Magnetic Resonance in Medicine, 2015, 73, 1505-1513.	3.0	49
64	Sexual Dimorphism in Hepatic, Adipose Tissue, and Peripheral Tissue Insulin Sensitivity in Obese Humans. Frontiers in Endocrinology, 2015, 6, 182.	3.5	48
65	The Effect of Spatial and Temporal Resolution of Cine Phase Contrast MRI on Wall Shear Stress and Oscillatory Shear Index Assessment. PLoS ONE, 2016, 11, e0163316.	2.5	47
66	Aortic valve stenosis and aortic diameters determine the extent of increased wall shear stress in bicuspid aortic valve disease. Journal of Magnetic Resonance Imaging, 2018, 48, 522-530.	3.4	47
67	Exploration of New Contrasts, Targets, and MR Imaging and Spectroscopy Techniques for Neuromuscular Disease – A Workshop Report of Working Group 3 of the Biomedicine and Molecular Biosciences COST Action BM1304 MYO-MRI. Journal of Neuromuscular Diseases, 2019, 6, 1-30.	2.6	46
68	Dynamic contrast-enhanced MRI in patients with luminal Crohn's disease. European Journal of Radiology, 2012, 81, 3019-3027.	2.6	45
69	Comparison of interobserver agreement of magnetic resonance elastography with histopathological staging of liver fibrosis. Abdominal Imaging, 2014, 39, 283-290.	2.0	45
70	White Matter Hyperintensity Volume and Cerebral Perfusion in Older Individuals with Hypertension Using Arterial Spin-Labeling. American Journal of Neuroradiology, 2016, 37, 1824-1830.	2.4	45
71	Liver Fibrosis in Type I Gaucher Disease: Magnetic Resonance Imaging, Transient Elastography and Parameters of Iron Storage. PLoS ONE, 2013, 8, e57507.	2.5	45
72	Visibility and artifacts of gold fiducial markers used for image guided radiation therapy of pancreatic cancer on MRI. Medical Physics, 2015, 42, 2638-2647.	3.0	44

#	Article	IF	CITATIONS
73	Feasibility and repeatability of PET with the hypoxia tracer [18F]HX4 in oesophageal and pancreatic cancer. Radiotherapy and Oncology, 2015, 116, 94-99.	0.6	44
74	Hyperthermia treatment planning for cervical cancer patients based on electrical conductivity tissue properties acquired <i>in vivo</i> with EPT at 3 T MRI. International Journal of Hyperthermia, 2016, 32, 558-568.	2.5	44
75	Comparison of six fit algorithms for the intra-voxel incoherent motion model of diffusion-weighted magnetic resonance imaging data of pancreatic cancer patients. PLoS ONE, 2018, 13, e0194590.	2.5	44
76	Measuring Wall Shear Stress Using Velocity-Encoded MRI. Current Cardiovascular Imaging Reports, 2014, 7, 1.	0.6	43
77	Threeâ€dimensional quantitative T <sub>1</sub> and T <sub>2</sub> mapping of the carotid artery: Sequence design and in vivo feasibility. Magnetic Resonance in Medicine, 2016, 75, 1008-1017.	3.0	43
78	Reversal of hepatic steatosis by omegaâ€3 fatty acids measured nonâ€invasively by <sup>1</sup> Hâ€magnetic resonance spectroscopy in a rat model. Journal of Gastroenterology and Hepatology (Australia), 2011, 26, 356-363.	2.8	42
79	Predictors of cerebral blood flow in patients with and without anemia. Journal of Applied Physiology, 2016, 120, 976-981.	2.5	42
80	Hepatic Insulin Resistance Is Not Pathway Selective in Humans With Nonalcoholic Fatty Liver Disease. Diabetes Care, 2021, 44, 489-498.	8.6	42
81	InÂVivo Imaging of Enhanced Leukocyte Accumulation in Atherosclerotic Lesions in Humans. Journal of the American College of Cardiology, 2014, 64, 1019-1029.	2.8	41
82	Relation between wall shear stress and carotid artery wall thickening MRI versus CFD. Journal of Biomechanics, 2016, 49, 735-741.	2.1	41
83	Improved unsupervised physicsâ€informed deep learning for intravoxel incoherent motion modeling and evaluation in pancreatic cancer patients. Magnetic Resonance in Medicine, 2021, 86, 2250-2265.	3.0	41
84	3D Cine Phase-Contrast MRI at 3T in Intracranial Aneurysms Compared with Patient-Specific Computational Fluid Dynamics. American Journal of Neuroradiology, 2013, 34, 1785-1791.	2.4	40
85	Review: Mechanical Characterization of Carotid Arteries and Atherosclerotic Plaques. IEEE Transactions on Ultrasonics, Ferroelectrics, and Frequency Control, 2016, 63, 1613-1623.	3.0	40
86	Hemodynamic provocation with acetazolamide shows impaired cerebrovascular reserve in adults with sickle cell disease. Haematologica, 2019, 104, 690-699.	3.5	40
87	White matter abnormalities in adults with 22q11 deletion syndrome with and without schizophrenia. Schizophrenia Research, 2011, 132, 75-83.	2.0	37
88	Proton Magnetic Resonance Spectroscopy in 22q11 Deletion Syndrome. PLoS ONE, 2011, 6, e21685.	2.5	37
89	Minimizing the Acquisition Time for Intravoxel Incoherent Motion Magnetic Resonance Imaging Acquisitions in the Liver and Pancreas. Investigative Radiology, 2016, 51, 211-220.	6.2	37
90	Abdominal organ motion during inhalation and exhalation breath-holds: pancreatic motion at different lung volumes compared. Radiotherapy and Oncology, 2016, 121, 268-275.	0.6	37

#	Article	IF	CITATIONS
91	In Vivo T1 of Blood Measurements in Children with Sickle Cell Disease Improve Cerebral Blood Flow Quantification from Arterial Spin-Labeling MRI. American Journal of Neuroradiology, 2016, 37, 1727-1732.	2.4	37
92	Cerebral Blood Flow Measurement in Children With Sickle Cell Disease Using Continuous Arterial Spin Labeling at 3.0-Tesla MRI. Stroke, 2009, 40, 795-800.	2.0	36
93	Disorganized Sensorimotor Integration in Mutation-Positive Myoclonus-Dystonia. Archives of Neurology, 2010, 67, 469-74.	4.5	35
94	Vessel wall characterization using quantitative MRI: what's in a number?. Magnetic Resonance Materials in Physics, Biology, and Medicine, 2018, 31, 201-222.	2.0	35
95	A novel MRI compatible soft tissue indentor and fibre Bragg grating force sensor. Medical Engineering and Physics, 2013, 35, 486-499.	1.7	34
96	Accuracy of abdominal ultrasound and MRI for detection of Crohn disease and ulcerative colitis in children. Pediatric Radiology, 2014, 44, 1370-1378.	2.0	33
97	Advanced cardiac MRI techniques for evaluation of leftâ€sided valvular heart disease. Journal of Magnetic Resonance Imaging, 2018, 48, 318-329.	3.4	33
98	Highly accelerated 4D flow cardiovascular magnetic resonance using a pseudo-spiral Cartesian acquisition and compressed sensing reconstruction for carotid flow and wall shear stress. Journal of Cardiovascular Magnetic Resonance, 2020, 22, 7.	3.3	33
99	MR Elastography of the Liver: Defining Thresholds for Detecting Viscoelastic Changes. Radiology, 2013, 269, 768-776.	7.3	32
100	Gray matter contamination in arterial spin labeling white matter perfusion measurements in patients with dementia. Neurolmage: Clinical, 2014, 4, 139-144.	2.7	32
101	Effect of Long-Term Vascular Care on Progression of Cerebrovascular Lesions. Stroke, 2017, 48, 1842-1848.	2.0	32
102	Emerging Magnetic Resonance Imaging Techniques for Atherosclerosis Imaging. Arteriosclerosis, Thrombosis, and Vascular Biology, 2019, 39, 841-849.	2.4	32
103	Acquisition Time and Reproducibility of Continuous Arterial Spin-Labeling Perfusion Imaging at 3T. American Journal of Neuroradiology, 2009, 30, 968-971.	2.4	31
104	Noninvasive quantification of hepatic steatosis inrats using 3.0 T <sup>1</sup> Hâ€magnetic resonance spectroscopy. Journal of Magnetic Resonance Imaging, 2010, 32, 148-154.	3.4	31
105	InÂVivo Imaging of Hypoxia in AtheroscleroticÂPlaques in Humans. JACC: Cardiovascular Imaging, 2015, 8, 1340-1341.	5.3	31
106	White matter has impaired resting oxygen delivery in sickle cell patients. American Journal of Hematology, 2019, 94, 467-474.	4.1	31
107	Cerebral oxygen metabolism in adults with sickle cell disease. American Journal of Hematology, 2020, 95, 401-412.	4.1	31
108	The Effect of a Diiodothyronine Mimetic on Insulin Sensitivity in Male Cardiometabolic Patients: A Double-Blind Randomized Controlled Trial. PLoS ONE, 2014, 9, e86890.	2.5	30

#	Article	IF	CITATIONS
109	Hepatic unsaturated fatty acids in patients with non-alcoholic fatty liver disease assessed by 3.0T MR spectroscopy. European Journal of Radiology, 2010, 75, e102-e107.	2.6	29
110	Robustness and Reproducibility of Flow Territories Defined by Planning-Free Vessel-Encoded Pseudocontinuous Arterial Spin-Labeling. American Journal of Neuroradiology, 2012, 33, E21-E25.	2.4	29
111	A novel diffusionâ€ŧensor <scp>MRI</scp> approach for skeletal muscle fascicle length measurements. Physiological Reports, 2016, 4, e13012.	1.7	29
112	Pseudo continuous arterial spin labeling quantification in anemic subjects with hyperemic cerebral blood flow. Magnetic Resonance Imaging, 2018, 47, 137-146.	1.8	29
113	Distinctive tics suppression network in Cilles de la Tourette syndrome distinguished from suppression of natural urges using multimodal imaging. NeuroImage: Clinical, 2018, 20, 783-792.	2.7	29
114	A tri-exponential model for intravoxel incoherent motion analysis of the human kidney: In silico and during pharmacological renal perfusion modulation. European Journal of Radiology, 2017, 91, 168-174.	2.6	28
115	Human Cardiac 31P-MR Spectroscopy at 3 Tesla Cannot Detect Failing Myocardial Energy Homeostasis during Exercise. Frontiers in Physiology, 2017, 8, 939.	2.8	28
116	Symptom validity testing in memory clinics: Hippocampal-memory associations and relevance for diagnosing mild cognitive impairment. Journal of Clinical and Experimental Neuropsychology, 2013, 35, 59-70.	1.3	27
117	A novel magnetic resonance elastography transducer concept based on a rotational eccentric mass: preliminary experiences with the gravitational transducer. Physics in Medicine and Biology, 2019, 64, 045007.	3.0	27
118	High Spatiotemporal Resolution 4D Flow MRI of Intracranial Aneurysms at 7T in 10 Minutes. American Journal of Neuroradiology, 2020, 41, 1201-1208.	2.4	27
119	Atherosclerosis imaging as a benchmark in the development of novel cardiovasular drugs. Current Opinion in Lipidology, 2007, 18, 613-621.	2.7	26
120	Endothelial Shear Stress. Circulation: Cardiovascular Imaging, 2010, 3, 578-585.	2.6	26
121	Cerebral Perfusion Long Term after Therapeutic Occlusion of the Internal Carotid Artery in Patients Who Tolerated Angiographic Balloon Test Occlusion. American Journal of Neuroradiology, 2012, 33, 329-335.	2.4	26
122	Additional Value of Intra-Aneurysmal Hemodynamics in Discriminating Ruptured versus Unruptured Intracranial Aneurysms. American Journal of Neuroradiology, 2015, 36, 1920-1926.	2.4	26
123	Use of Antiplatelet Agents Is Associated With Intraplaque Hemorrhage on Carotid Magnetic Resonance Imaging. Stroke, 2015, 46, 3411-3415.	2.0	26
124	Increased arterial wall inflammation in patients with ankylosing spondylitis is reduced by statin therapy. Annals of the Rheumatic Diseases, 2016, 75, 1848-1851.	0.9	26
125	Assessment of Imaging Modalities Against Liver Biopsy in Nonalcoholic Fatty Liver Disease: The Amsterdam <scp>NAFLDâ€NASH</scp> Cohort. Journal of Magnetic Resonance Imaging, 2021, 54, 1937-1949.	3.4	26
126	Dopaminergic System Dysfunction in Recreational Dexamphetamine Users. Neuropsychopharmacology, 2015, 40, 1172-1180.	5.4	25

#	Article	IF	CITATIONS
127	Risk factor analysis of cerebral white matter hyperintensities in children with sickle cell disease. British Journal of Haematology, 2016, 172, 274-284.	2.5	25
128	Diffusionâ€prepared stimulatedâ€echo turbo spin echo (DPstiâ€TSE): An eddy currentâ€insensitive sequence for threeâ€dimensional highâ€resolution and undistorted diffusionâ€weighted imaging. NMR in Biomedicine, 2017, 30, e3719.	2.8	25
129	Comparison of Velocity- and Acceleration-Selective Arterial Spin Labeling with [ <sup>15</sup> 0]H <sub>2</sub> 0 Positron Emission Tomography. Journal of Cerebral Blood Flow and Metabolism, 2015, 35, 1296-1303.	4.3	24
130	Breast magnetic resonance elastography: a review of clinical work and future perspectives. NMR in Biomedicine, 2018, 31, e3932.	2.8	24
131	Plaque Permeability Assessed With DCE-MRI Associates With USPIO Uptake inÂPatients With Peripheral Artery Disease. JACC: Cardiovascular Imaging, 2019, 12, 2081-2083.	5.3	24
132	Comparison of Phase-Contrast MR Imaging and Endovascular Sonography for Intracranial Blood Flow Velocity Measurements. American Journal of Neuroradiology, 2012, 33, 1786-1790.	2.4	23
133	Use of continuously MR tagged imaging for automated motion assessment in the abdomen: A feasibility study. Journal of Magnetic Resonance Imaging, 2012, 36, 492-497.	3.4	23
134	Functional MRI study of response inhibition in myoclonus dystonia. Experimental Neurology, 2013, 247, 623-629.	4.1	23
135	Magnetic Resonance Imaging–Derived Renal Oxygenation and Perfusion During Continuous, Steady‣tate Angiotensinâ€II Infusion inÂHealthy Humans. Journal of the American Heart Association, 2016, 5, e003185.	3.7	23
136	Addition of MRI for CT-based pancreatic tumor delineation: a feasibility study. Acta Oncológica, 2017, 56, 923-930.	1.8	23
137	An iterative sparse deconvolution method for simultaneous multicolor <sup>19</sup> Fâ€MRI of multiple contrast agents. Magnetic Resonance in Medicine, 2020, 83, 228-239.	3.0	23
138	Quantitative MRI Reveals Microstructural Changes in the Upper Leg Muscles After Running a Marathon. Journal of Magnetic Resonance Imaging, 2020, 52, 407-417.	3.4	23
139	Pathological validation and prognostic potential of quantitative MRI in the characterization of pancreas cancer: preliminary experience. Molecular Oncology, 2020, 14, 2176-2189.	4.6	23
140	Quantitative perfusion mapping with induced transient hypoxia using BOLD MRI. Magnetic Resonance in Medicine, 2021, 85, 168-181.	3.0	23
141	Reliability of in vivo determination of forearm muscle volume using 3.0 T magnetic resonance imaging. Journal of Magnetic Resonance Imaging, 2010, 31, 1252-1255.	3.4	22
142	Validation of continuously tagged MRI for the measurement of dynamic 3D skeletal muscle tissue deformation. Medical Physics, 2012, 39, 1793-1810.	3.0	21
143	Increasing spatial resolution of 3T MRI scanning improves reproducibility of carotid arterial wall dimension measurements. Magnetic Resonance Materials in Physics, Biology, and Medicine, 2014, 27, 219-226.	2.0	21
144	No benefit of HDL mimetic CER-001 on carotid atherosclerosis in patients with genetically determined very low HDL levels. Atherosclerosis, 2020, 311, 13-19.	0.8	21

#	Article	IF	CITATIONS
145	Juvenile Idiopathic Arthritis: Diffusion-weighted MRI in the Assessment of Arthritis in the Knee. Radiology, 2020, 295, 373-380.	7.3	21
146	Noninvasive automated motion assessment of intestinal motility by continuously tagged MR imaging. Journal of Magnetic Resonance Imaging, 2014, 39, 9-16.	3.4	20
147	Cerebral Lesions on 7 Tesla MRI in Patients with Sickle Cell Anemia. Cerebrovascular Diseases, 2015, 39, 181-189.	1.7	20
148	Accelerated 4 <scp>D</scp> phase contrast <scp>MRI</scp> in skeletal muscle contraction. Magnetic Resonance in Medicine, 2018, 80, 1799-1811.	3.0	20
149	Evaluation of Six Diffusion-weighted MRI Models for Assessing Effects of Neoadjuvant Chemoradiation in Pancreatic Cancer Patients. International Journal of Radiation Oncology Biology Physics, 2018, 102, 1052-1062.	0.8	20
150	Effects of systematic partial volume errors on the estimation of gray matter cerebral blood flow with arterial spin labeling MRI. Magnetic Resonance Materials in Physics, Biology, and Medicine, 2018, 31, 725-734.	2.0	20
151	Reduced global cerebral oxygen metabolic rate in sickle cell disease and chronic anemias. American Journal of Hematology, 2021, 96, 901-913.	4.1	20
152	Quantitative Functional Arterial Spin Labeling (fASL) MRI – Sensitivity and Reproducibility of Regional CBF Changes Using Pseudo-Continuous ASL Product Sequences. PLoS ONE, 2015, 10, e0132929.	2.5	20
153	Measuring liver triglyceride content in mice: non-invasive magnetic resonance methods as an alternative to histopathology. Magnetic Resonance Materials in Physics, Biology, and Medicine, 2014, 27, 317-327.	2.0	19
154	Diffusion Tensor MRI of the Heart – In Vivo Imaging of Myocardial Fiber Architecture. Current Cardiovascular Imaging Reports, 2014, 7, 1.	0.6	19
155	Clinical intra-cardiac 4D flow CMR: acquisition, analysis, and clinical applications. European Heart Journal Cardiovascular Imaging, 2022, 23, 154-165.	1.2	19
156	Hepatic Steatosis in Morbidly Obese Patients Undergoing Gastric Bypass Surgery: Assessment With Open-System <sup>1</sup> H-MR Spectroscopy. American Journal of Roentgenology, 2011, 196, W736-W742.	2.2	18
157	Feasibility of ASL-based phMRI with a single dose of oral citalopram for repeated assessment of serotonin function. NeuroImage, 2012, 63, 1695-1700.	4.2	18
158	Mapping the hemodynamic response in human subjects to a dopaminergic challenge with dextroamphetamine using ASL-based pharmacological MRI. NeuroImage, 2013, 72, 1-9.	4.2	18
159	MRI strain imaging of the carotid artery: Present limitations and future challenges. Journal of Biomechanics, 2014, 47, 824-833.	2.1	18
160	Myocardial Injury and Compromised Cardiomyocyte Integrity Following a Marathon Run. JACC: Cardiovascular Imaging, 2020, 13, 1445-1447.	5.3	18
161	Investigations of Carotid Stenosis to Identify Vulnerable Atherosclerotic Plaque and Determine Individual Stroke Risk. Circulation Journal, 2017, 81, 1246-1253.	1.6	17
162	Dynamic MRI for bowel motility imaging–how fast and how long?. British Journal of Radiology, 2018, 91, 20170845.	2.2	17

#	Article	IF	CITATIONS
163	Regional assessment of carotid artery pulse wave velocity using compressed sensing accelerated high temporal resolution 2D CINE phase contrast cardiovascular magnetic resonance. Journal of Cardiovascular Magnetic Resonance, 2018, 20, 86.	3.3	17
164	Diffusion tensor MRI of the healthy brachial plexus. PLoS ONE, 2018, 13, e0196975.	2.5	17
165	Pseudoâ€spiral sampling and compressed sensing reconstruction provides flexibility of temporal resolution in accelerated aortic 4D flow MRI: A comparison with kâ€ŧ principal component analysis. NMR in Biomedicine, 2020, 33, e4255.	2.8	17
166	Calibration of T <sub>2</sub> oximetry MRI for subjects with sickle cell disease. Magnetic Resonance in Medicine, 2021, 86, 1019-1028.	3.0	17
167	Deep learning DCE-MRI parameter estimation: Application in pancreatic cancer. Medical Image Analysis, 2022, 80, 102512.	11.6	17
168	Monoaminergic dysfunction in recreational users of dexamphetamine. European Neuropsychopharmacology, 2013, 23, 1491-1502.	0.7	16
169	Repeatability of in vivo quantification of atherosclerotic carotid artery plaque components by supervised multispectral classification. Magnetic Resonance Materials in Physics, Biology, and Medicine, 2015, 28, 535-545.	2.0	16
170	Repeatability and correlations of dynamic contrast enhanced and T2* MRI in patients with advanced pancreatic ductal adenocarcinoma. Magnetic Resonance Imaging, 2018, 50, 1-9.	1.8	16
171	Aneurysmal Parent Artery–Specific Inflow Conditions for Complete and Incomplete Circle of Willis Configurations. American Journal of Neuroradiology, 2018, 39, 910-915.	2.4	16
172	An advanced magnetic resonance imaging perspective on the etiology of deep tissue injury. Journal of Applied Physiology, 2018, 124, 1580-1596.	2.5	16
173	Impairment of Cerebrovascular Hemodynamics in Patients With Severe and Milder Forms of Sickle Cell Disease. Frontiers in Physiology, 2021, 12, 645205.	2.8	16
174	A MRI-Compatible Combined Mechanical Loading and MR Elastography Setup to Study Deformation-Induced Skeletal Muscle Damage in Rats. PLoS ONE, 2017, 12, e0169864.	2.5	16
175	Longitudinal relation between blood pressure, antihypertensive use and cerebral blood flow, using arterial spin labelling MRI. Journal of Cerebral Blood Flow and Metabolism, 2021, 41, 1756-1766.	4.3	16
176	Nonalcoholic fatty liver disease and cardiovascular risk in children with obesity. Obesity, 2015, 23, 1239-1243.	3.0	15
177	Multiscale 3-D + <i>t</i> Intracranial Aneurysmal Flow Vortex Detection. IEEE Transactions on Biomedical Engineering, 2015, 62, 1355-1362.	4.2	15
178	Learningâ€based automated segmentation of the carotid artery vessel wall in dualâ€sequence MRI using subdivision surface fitting. Medical Physics, 2017, 44, 5244-5259.	3.0	15
179	Validation of SPAMM tagged MRI based measurement of 3D soft tissue deformation. Medical Physics, 2011, 38, 1248-1260.	3.0	14
180	Whole heart DTI using asymmetric bipolar diffusion gradients. Journal of Cardiovascular Magnetic Resonance, 2015, 17, P15.	3.3	14

#	Article	IF	CITATIONS
181	Diffusionâ€prepared neurography of the brachial plexus with a large fieldâ€ofâ€view at 3T. Journal of Magnetic Resonance Imaging, 2016, 43, 644-654.	3.4	14
182	Comparison of clinical MRI liver iron content measurements using signal intensity ratios, R 2 and R 2*. Abdominal Radiology, 2016, 41, 2123-2131.	2.1	14
183	Assessment of passive muscle elongation using Diffusion Tensor MRI: Correlation between fiber length and diffusion coefficients. NMR in Biomedicine, 2016, 29, 1813-1824.	2.8	14
184	Intracranial 4D flow magnetic resonance imaging reveals altered haemodynamics in sickle cell disease. British Journal of Haematology, 2018, 180, 432-442.	2.5	14
185	Magnetic resonance elastography of skeletal muscle deep tissue injury. NMR in Biomedicine, 2019, 32, e4087.	2.8	14
186	Glycerophosphocholine and Glycerophosphoethanolamine Are Not the Main Sources of the In Vivo31P MRS Phosphodiester Signals from Healthy Fibroglandular Breast Tissue at 7 T. Frontiers in Oncology, 2016, 6, 29.	2.8	13
187	Accelerated 4D selfâ€gated MRI of tibiofemoral kinematics. NMR in Biomedicine, 2017, 30, e3791.	2.8	13
188	Dynamic magnetic resonance measurements of calf muscle oxygenation and energy metabolism in peripheral artery disease. Journal of Magnetic Resonance Imaging, 2020, 51, 98-107.	3.4	13
189	Quantification of Mitral Valve Regurgitation from 4D Flow MRI Using Semiautomated Flow Tracking. Radiology: Cardiothoracic Imaging, 2020, 2, e200004.	2.5	13
190	Cerebral Blood Flow in Patients with Severe Aortic Valve Stenosis Undergoing Transcatheter Aortic Valve Implantation. Journal of the American Geriatrics Society, 2021, 69, 494-499.	2.6	13
191	Detection of Liquid Phase Cholesteryl Ester in Carotid Atherosclerosis by 1H-MR Spectroscopy in Humans. JACC: Cardiovascular Imaging, 2013, 6, 1277-1284.	5.3	12
192	Aortic valve calcification volumes and chronic brain infarctions in patients undergoing transcatheter aortic valve implantation. International Journal of Cardiovascular Imaging, 2019, 35, 2123-2133.	1.5	12
193	Semi-quantitative cerebral blood flow parameters derived from non-invasive [ <sup>15</sup> 0]H <sub>2</sub> 0 PET studies. Journal of Cerebral Blood Flow and Metabolism, 2019, 39, 163-172.	4.3	12
194	The repeatability of bilateral diffusion tensor imaging (DTI) in the upper leg muscles of healthy adults. European Radiology, 2020, 30, 1709-1718.	4.5	12
195	Fully quantitative mapping of abnormal aortic velocity and wall shear stress direction in patients with bicuspid aortic valves and repaired coarctation using 4D flow cardiovascular magnetic resonance. Journal of Cardiovascular Magnetic Resonance, 2021, 23, 9.	3.3	12
196	Carriers of Loss-of-Function Mutations in EXT Display Impaired Pancreatic Beta-Cell Reserve Due to Smaller Pancreas Volume. PLoS ONE, 2014, 9, e115662.	2.5	12
197	B1-based SAR reconstruction using contrast source inversion–electric properties tomography (CSI-EPT). Medical and Biological Engineering and Computing, 2017, 55, 225-233.	2.8	11
198	Four-dimensional flow MRI of stented versus stentless aortic valve bioprostheses. European Radiology, 2018, 28, 257-264.	4.5	11

#	Article	IF	CITATIONS
199	Spatial correlations between MRI-derived wall shear stress and vessel wall thickness in the carotid bifurcation. European Radiology Experimental, 2018, 2, 27.	3.4	11
200	Crossing muscle fibers of the human tongue resolved in vivo using constrained spherical deconvolution. Journal of Magnetic Resonance Imaging, 2019, 50, 96-105.	3.4	11
201	Detecting the effects of a standardized meal challenge on small bowel motility with MRI in prepared and unprepared bowel. Neurogastroenterology and Motility, 2019, 31, e13506.	3.0	11
202	Quantification of cerebral perfusion and cerebrovascular reserve using Turboâ€QUASAR arterial spin labeling MRI. Magnetic Resonance in Medicine, 2020, 83, 731-748.	3.0	11
203	Assessment of fasted and fed gastrointestinal contraction frequencies in healthy subjects using continuously tagged MRI. Neurogastroenterology and Motility, 2020, 32, e13747.	3.0	11
204	Subclinical effects of longâ€chain fatty acid βâ€oxidation deficiency on the adult heart: A caseâ€control magnetic resonance study. Journal of Inherited Metabolic Disease, 2020, 43, 969-980.	3.6	11
205	Gender- and Age-Associated Differences in Bone Marrow Adipose Tissue and Bone Marrow Fat Unsaturation Throughout the Skeleton, Quantified Using Chemical Shift Encoding-Based Water–Fat MRI. Frontiers in Endocrinology, 2022, 13, 815835.	3.5	11
206	Feasibility of using automated insufflated carbon dioxide (CO2) for luminal distension in 3.0T MR colonography. European Journal of Radiology, 2012, 81, 1128-1133.	2.6	10
207	MRI-based biomechanical parameters for carotid artery plaque vulnerability assessment. Thrombosis and Haemostasis, 2016, 115, 493-500.	3.4	10
208	Quantitative agreement between [ <sup>15</sup> 0]H <sub>2</sub> 0 PET and model free QUASAR MRIâ€derived cerebral blood flow and arterial blood volume. NMR in Biomedicine, 2016, 29, 519-526.	2.8	10
209	In Vivo Reconstruction of Lumbar Erector Spinae Architecture Using Diffusion Tensor MRI. Clinical Spine Surgery, 2016, 29, E139-E145.	1.3	10
210	Late-life brain perfusion after prenatal famine exposure. Neurobiology of Aging, 2019, 82, 1-9.	3.1	10
211	T1ï•mapping for assessing knee joint cartilage in children with juvenile idiopathic arthritis — feasibility and repeatability. Pediatric Radiology, 2020, 50, 371-379.	2.0	10
212	Effects of Acquisition Parameter Modifications and Field Strength on the Reproducibility of Brain Perfusion Measurements Using Arterial Spin-Labeling. American Journal of Neuroradiology, 2021, 42, 109-115.	2.4	10
213	Reproducibility of pharmacological ASL using sequences from different vendors: implications for multicenter drug studies. Magnetic Resonance Materials in Physics, Biology, and Medicine, 2015, 28, 427-436.	2.0	9
214	Quantification of Myocardial Creatine and Triglyceride Content in the Human Heart: Precision and Accuracy of in vivo Proton Magnetic Resonance Spectroscopy. Journal of Magnetic Resonance Imaging, 2021, 54, 411-420.	3.4	9
215	Comparison of In Vivo Carotid 3.0-T Magnetic Resonance to B-Mode Ultrasound Imaging and Histology in a Porcine Model. JACC: Cardiovascular Imaging, 2009, 2, 744-750.	5.3	8
216	Increasing the Spatial Resolution of 3T Carotid MRI Has No Beneficial Effect for Plaque Component Measurement Reproducibility. PLoS ONE, 2015, 10, e0130878.	2.5	8

#	Article	IF	CITATIONS
217	An isolated beating pig heart platform for a comprehensive evaluation of intracardiac blood flow with 4D flow MRI: a feasibility study. European Radiology Experimental, 2019, 3, 40.	3.4	8
218	Threeâ€dimensional diffusion imaging with spiral encoded navigators from stimulated echoes (3Dâ€ÐISPENSE). Magnetic Resonance in Medicine, 2019, 81, 1052-1065.	3.0	8
219	Quantitative Determination of Liver Triglyceride Levels with 3T 1H-MR Spectroscopy in Mice with Moderately Elevated Liver Fat Content. Academic Radiology, 2014, 21, 1446-1454.	2.5	7
220	A new murine model to study musculoskeletal tuberculosis (short communication). Tuberculosis, 2014, 94, 306-310.	1.9	7
221	Quantitative assessment of biliary stent artifacts on MR images: Potential implications for target delineation in radiotherapy. Medical Physics, 2016, 43, 5603-5615.	3.0	7
222	MRI based 3D finite element modelling to investigate deep tissue injury. Computer Methods in Biomechanics and Biomedical Engineering, 2018, 21, 760-769.	1.6	7
223	Bileaflet mechanical aortic valves do not alter ascending aortic wall shear stress. International Journal of Cardiovascular Imaging, 2019, 35, 703-710.	1.5	7
224	<b>Inherently decoupled</b> <sup><b>1</b></sup> <b>H antennas and</b> <sup><b>31</b></sup> <bp 7="" at="" b="" for="" imaging="" liver="" loops="" metabolic="" metastasis="" of="" t<="">. NMR in Biomedicine, 2020, 33, e4221.</bp>	2.8	7
225	Phase I/II Study of LDE225 in Combination with Gemcitabine and Nab-Paclitaxel in Patients with Metastatic Pancreatic Cancer. Cancers, 2021, 13, 4869.	3.7	7
226	Reduced Cerebral Metabolic Rate of Oxygen in Adults with Sickle Cell Disease. Blood, 2018, 132, 11-11.	1.4	7
227	Manual versus Automated Carotid Artery Plaque Component Segmentation in High and Lower Quality 3.0 Tesla MRI Scans. PLoS ONE, 2016, 11, e0164267.	2.5	7
228	A Distributed Workflow Management System for Automated Medical Image Analysis and Logistics. , 2006, , .		6
229	Magnetic resonance colonography with automated carbon dioxide insufflation: Diagnostic accuracy and distension. European Journal of Radiology, 2014, 83, 743-750.	2.6	6
230	Magnetic resonance colonography with a limited bowel preparation and automated carbon dioxide insufflation in comparison to conventional colonoscopy: Patient burden and preferences. European Journal of Radiology, 2015, 84, 19-25.	2.6	6
231	Impact of Structural Cerebral Damage in Adults With Tetralogy of Fallot. Circulation, 2017, 135, 1873-1875.	1.6	6
232	Animal studies in clinical MRI scanners: A custom setup for combined fMRI and deep-brain stimulation in awake rats. Journal of Neuroscience Methods, 2021, 360, 109240.	2.5	6
233	Comparative Analysis of Blood <scp>T<sub>2</sub></scp> Values Measured by <scp>T<sub>2</sub>â€TRIR</scp> and <scp>TRUST</scp> . Journal of Magnetic Resonance Imaging, 2022, 56, 516-526.	3.4	6
234	Thoracic aortic wall shear stress atlases in patients with bicuspid aortic valves. Journal of Cardiovascular Magnetic Resonance, 2014, 16, P161.	3.3	5

#	Article	IF	CITATIONS
235	Water and fat separation in realâ€time MRI of joint movement with phaseâ€sensitive bSSFP. Magnetic Resonance in Medicine, 2017, 78, 58-68.	3.0	5
236	Prospective validation of craniocaudal tumour size on MR imaging compared to histoPAthology in patients with uterine cervical cancer: The MPAC study. Clinical and Translational Radiation Oncology, 2019, 18, 9-15.	1.7	5
237	Supervised segmentation framework for evaluation of diffusion tensor imaging indices in skeletal muscle. NMR in Biomedicine, 2021, 34, e4406.	2.8	5
238	Retrospective Cameraâ€Based Respiratory Gating in Clinical Wholeâ€Heart 4D Flow MRI. Journal of Magnetic Resonance Imaging, 2021, 54, 440-451.	3.4	5
239	Cardiac Biomarker Kinetics and Their Association With Magnetic Resonance Measures of Cardiomyocyte Integrity Following a Marathon Run: Implications for Postexercise Biomarker Testing. Journal of the American Heart Association, 2021, 10, e020039.	3.7	5
240	Marathon running transiently depletes the myocardial lipid pool. Physiological Reports, 2020, 8, e14543.	1.7	5
241	Anemia Increases Oxygen Extraction Fraction in Deep Brain Structures but Not in the Cerebral Cortex. Frontiers in Physiology, 0, 13, .	2.8	5
242	Guideline treatment results in regression of atherosclerosis in type 2 diabetes mellitus. Diabetes and Vascular Disease Research, 2015, 12, 126-132.	2.0	4
243	Revisiting the Potential of Alternating Repetition Time Balanced Steady-State Free Precession Imaging of the Abdomen at 3 T. Investigative Radiology, 2016, 51, 560-568.	6.2	4
244	2D AMESING multi-echo 31P-MRSI of the liver at 7T allows transverse relaxation assessment and T2-weighted averaging for improved SNR. Magnetic Resonance Imaging, 2016, 34, 219-226.	1.8	4
245	Comparison of four MR carotid surface coils at 3T. PLoS ONE, 2019, 14, e0213107.	2.5	4
246	Abnormal blood flow and wall shear stress are present in corrected aortic coarctation despite successful surgical repair. Journal of Cardiovascular Surgery, 2019, 60, 152-154.	0.6	4
247	Sympathetic activation by lower body negative pressure decreases kidney perfusion without inducing hypoxia in healthy humans. Clinical Autonomic Research, 2020, 30, 149-156.	2.5	4
248	The road to optimal acceleration of Dixon imaging and quantitative T2-mapping in the ankle using compressed sensing and parallel imaging. European Journal of Radiology, 2020, 132, 109295.	2.6	4
249	A 12-channel flexible receiver coil for accelerated tongue imaging. Magnetic Resonance Materials in Physics, Biology, and Medicine, 2020, 33, 581-590.	2.0	4
250	<scp>Wholeâ€Heart 4D</scp> Flow <scp>MRI</scp> for Evaluation of Normal and Regurgitant Valvular Flow: A Quantitative Comparison Between <scp>Pseudoâ€Spiral</scp> Sampling and <scp>EPI</scp> Readout. Journal of Magnetic Resonance Imaging, 2022, 55, 1120-1130.	3.4	4
251	A scale space based algorithm for automated segmentation of single shot tagged MRI of shearing deformation. Magnetic Resonance Materials in Physics, Biology, and Medicine, 2013, 26, 229-238.	2.0	3
252	Endothelial shear stress estimation in the human carotid artery based on Womersley versus Poiseuille flow. International Journal of Cardiovascular Imaging, 2015, 31, 585-593.	1.5	3

#	Article	IF	CITATIONS
253	Compressed sensing MRI with variable density averaging (CS-VDA) outperforms full sampling at low SNR. Physics in Medicine and Biology, 2020, 65, 045004.	3.0	3
254	Double delay alternating with nutation for tailored excitation facilitates bandingâ€free isotropic highâ€resolution intracranial vessel wall imaging. NMR in Biomedicine, 2021, 34, e4567.	2.8	3
255	Coronary Flow Assessment Using Accelerated 4D Flow MRI With Respiratory Motion Correction. Frontiers in Bioengineering and Biotechnology, 2021, 9, 725833.	4.1	3
256	Ultra-high resolution, 3-dimensional magnetic resonance imaging of the atherosclerotic vessel wall at clinical 7T. PLoS ONE, 2020, 15, e0241779.	2.5	3
257	Multiâ€parametric quantitative magnetic resonance imaging of the upper arm muscles of patients with spinal muscular atrophy. NMR in Biomedicine, 2022, 35, e4696.	2.8	3
258	Volume of White Matter Hyperintensities Predicts Neurocognitive Functioning in Children with Sickle Cell Disease. Blood, 2014, 124, 2720-2720.	1.4	2
259	Locally advanced rectal cancer: 3D diffusion-prepared stimulated-echo turbo spin-echo versus 2D diffusion-weighted echo-planar imaging. European Radiology Experimental, 2020, 4, 9.	3.4	2
260	Cerebral Blood Flow Measurement in Children with Sickle Cell Disease Using CASL at 3.0 Tesla MRI. Blood, 2008, 112, 711-711.	1.4	2
261	Cerebral Small Vessel Disease In Patients With Sickle Cell Disease: Initial Findings With Ultra-High Field 7T MRI. Blood, 2013, 122, 1011-1011.	1.4	2
262	Dynamic MRI of swallowing: real-time volumetric imaging at 12 frames per second at 3ÂT. Magnetic Resonance Materials in Physics, Biology, and Medicine, 2022, 35, 411-419.	2.0	2
263	Dynamic MR imaging of cerebral perfusion during bicycling exercise. NeuroImage, 2022, 250, 118961.	4.2	2
264	Advanced cardiac MRI techniques for evaluation of left-sided valvular heart disease. Journal of Magnetic Resonance Imaging, 2018, 48, spcone-spcone.	3.4	1
265	Data Assimilation for Full 4D PCâ€MRI Measurements: Physicsâ€Based Denoising and Interpolation. Computer Graphics Forum, 2020, 39, 496-512.	3.0	1
266	Carotid plaque composition in persons with hemophilia: An explorative study with multi-contrast MRI. Thrombosis Research, 2021, 197, 138-140.	1.7	1
267	Reduced Cerebrovascular Reserve Capacity in Adults with Sickle Cell Disease. Blood, 2017, 130, 972-972.	1.4	1
268	A diffusion tensor-based method facilitating volumetric assessment of fiber orientations in skeletal muscle. PLoS ONE, 2022, 17, e0261777.	2.5	1
269	Longitudinal CMR assessment of cardiac global longitudinal strain and hemodynamic forces in a mouse model of heart failure. International Journal of Cardiovascular Imaging, 2022, 38, 2385-2394.	0.6	1
270	Diffusion-tensor MRI reveals the complex muscle architecture of the human forearm. Journal of Magnetic Resonance Imaging, 2012, 36, spcone-spcone.	3.4	0

#	Article	IF	CITATIONS
271	Cerebral imaging with 7-Tesla MRI in patients with sickle cell disease: a pilot study. Tijdschrift Voor Kindergeneeskunde, 2013, 81, 76-76.	0.0	0
272	Evaluating intensity normalization for multispectral classification of carotid atherosclerotic plaque. , 2015, , .		0
273	SP224TRIâ <sup>~</sup> 'EXPONENTIAL APPROACH FOR INTRAVOXEL INCOHERENT MOTION ANALYSISOF MULTI Bâ <sup>~</sup> 'VALUE DIFFUSION WHEIGTED MRI DATA FOLLOWS GFR CHANGES IN HEALTHY HUMANS. Nephrology Dialysis Transplantation, 2016, 31, i161-i161.	0.7	0
274	The Authors Reply:. JACC: Cardiovascular Imaging, 2020, 13, 2063-2064.	5.3	0
275	Re: Estimating the Population-level Effectiveness of Vaccination Programs in the Netherlands. Epidemiology, 2020, 31, e27-e29.	2.7	0
276	Editorial for "Quantification of Regional Cerebral Blood Flow Using Diffusion Imaging With <scp>Phase ontrast</scp> ― Journal of Magnetic Resonance Imaging, 2021, 54, 1687-1688.	3.4	0
277	SAT0644â€T1rho mapping in the assessment of articular cartilage integrity of the knee in children with juvenile idiopathic arthritis. , 2018, , .		0
278	Hinge point fibrosis is highly prevalent in male elite water polo players. European Heart Journal, 2020, 41, .	2.2	0
279	The relationship between quantitative magnetic resonance imaging of the ankle plantar flexors, muscle function during walking and maximal strength in people with neuromuscular diseases. Clinical Biomechanics, 2022, 94, 105609.	1.2	0
280	Aortic dilatation using cardiac magnetic resonance in asymptomatic ELITE athletes. European Journal of Preventive Cardiology, 2022, 29, .	1.8	0
281	Late gadolinium enhancement of the hinge point is a common finding in asymptomatic ELITE athletes. European Journal of Preventive Cardiology, 2022, 29, .	1.8	0